# Selective Filtering of Particles by the Extracellular Matrix: An Electrostatic Bandpass

Oliver Lieleg,[†‡*] Regina M. Baumgärtel,[†] and Andreas R. Bausch[†*]
[†]Lehrstuhl für Zellbiophysik E27, Technische Universität München, Garching, Germany; and [‡]Faculty of Arts and Sciences, Center for Systems Biology, Harvard University, Cambridge, Massachusetts

ABSTRACT The transport of microscopic particles such as growth factors, proteins, or drugs through the extracellular matrix (ECM) is based on diffusion, a ubiquitous mechanism in nature. The ECM shapes the local distribution of the transported macromolecules and at the same time constitutes an important barrier toward infectious agents. To fulfill these competing tasks, the hydrogels have to employ highly selective filtering mechanisms. Yet, the underlying microscopic principles are still an enigma in cell biology and drug delivery. Here, we show that the extracellular matrix presents an effective electrostatic bandpass, suppressing the diffusive motion of both positively and negatively charged objects. This mechanism allows uncharged particles to easily diffuse through the matrix, while charged particles are effectively trapped. However, by tuning the strength of this physical interaction of the particles with the biopolymer matrix, the microscopic mobility of formerly trapped particles can be rescued on demand. Moreover, we identify heparan sulfate chains to be one important key factor for the barrier function of the extracellular matrix. We propose that localized charge patches in the ECM are responsible for its highly unspecific but strongly selective filtering effect. Such localized interactions could also account for the observed tunability and selectivity of many other important permeability barriers that are established by biopolymer-based hydrogels, e.g., the mucus layer of endothelial cells or the hydrogel in the nuclear core complex.

## INTRODUCTION

Many prokaryotic and eukaryotic cells are embedded in hydrogels comprising different biopolymers and proteoglycans that fill the extracellular space. These hydrogels provide mechanical support, shield the cells from their environment, and separate different types of tissue. Depending on the particular function of the extracellular hydrogel, different cell types have developed tailored extracellular matrix (ECM) systems with distinct compositions of biopolymers. Tenascin, laminin, vitronectin, fibronectin, and collagens are prominent examples of such extracellular biopolymers (1), which differ not only in their biophysical properties but also in their biochemical architecture. In the basal lamina, the extracellular matrix consists of the three biopolymers laminin, collagen IV, and heparan sulfate (2), the latter of which is organized in the perlecan complex. Nidogen acts as a cross-linking molecule between these biopolymers (Fig. 1 *A*), and is thought to maintain the spatial relationship between laminin and collagen IV (3). This polymer-based microenvironment not only stimulates cell adhesion and proliferation, but is crucial, also, for the correct communication between different cells in both tissue development and maintenance (4). Here, cells rely on the proper transport of small molecules such as growth factors (5), which is mainly achieved by diffusion. Moreover, the extracellular matrix shapes and regulates the distribution of many other diffusing proteins, ions, and drugs (6). In tumor tissue, this microscopic filtering process is malfunctioning, giving rise to an increased barrier function of the ECM (1).

As outlined by several studies, smaller particles can penetrate this barrier more efficiently than large particles (7,8). Thus, it was suggested that the main contribution to the barrier function of the ECM arises from the density of the biopolymer meshwork (9). However, for particles that are smaller than the mesh size of the ECM, the barrier function of the extracellular matrix cannot be based on size exclusion effects. Instead, alternative filtering mechanisms have to be employed. For this purpose, the surface charge of the particles might play an important role as, e.g., reported for the blood-brain-barrier (10) and from tumor treatment studies (11). Indeed, some earlier works proposed that proteoglycans create a permeability barrier inside the basement membrane that blocks the passage of negatively charged macromolecules (12,13). Yet, while the biochemical composition of extracellular matrix systems is well understood by now, a systematic investigation of the filtering properties of ECM hydrogels and an identification of the underlying microscopic principles is still lacking.

In this study, we investigate the selective filter mechanism of extracellular matrix hydrogels, which are reconstituted from the basement membrane of mice. We analyze the microscopic mobility of various test particles, which differ in size and surface charge, to disentangle the contribution of these two physical parameters to the filtering mechanism of the ECM. We show that the extracellular matrix acts as an electrostatic bandpass: Charged particles can only diffuse within the ECM as long as their surface charge does not exceed a well-defined window. The mobility of highly

*Submitted May 8, 2009, and accepted for publication July 8, 2009.*

*Correspondence: olieleg@cgr.harvard.edu or abausch@ph.tum.de

Editor: Denis Wirtz.



0006-3495/09/09/1569/9 $2.00

doi: 10.1016/j.bpj.2009.07.009

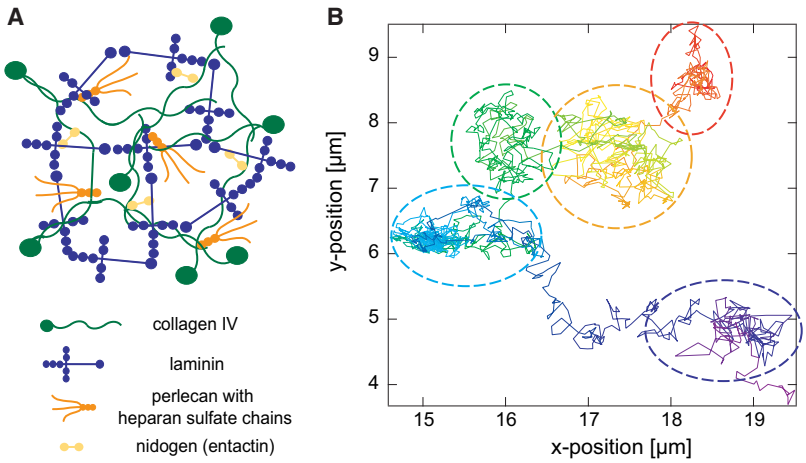


FIGURE 1 Architecture of the extracellular matrix. (*A*) The extracellular matrix in the basal lamina is composed of three biopolymers: laminin, collagen IV, and heparan sulfate molecules, which are organized in the perlecan complex. These biopolymers are interconnected to each other by nidogen. (*B*) Trajectory of a PEG-passivated polystyrene bead of 1.1 $\mu$m size in an ECM hydrogel for a time range of 60 s. The temporal evolution of the particle position is encoded in the color scheme. The particle travels several meshes of the hydrogel, which appear to have a typical size of $\approx$2–3 $\mu$m.

charged particles of both algebraic signs is drastically reduced to virtually zero even though the particles are significantly smaller than the mesh size of the ECM hydrogel. However, the mobility of the trapped particles can be rescued if their surface charge is effectively shielded. We demonstrate that heparan sulfate chains, which are immobilized to the protein network of the hydrogel, are essential for this highly selective but unspecific barrier function of the ECM.

## MATERIALS AND METHODS

### Proteins and particles

#### *Proteins*

All proteins and enzymes were obtained from Sigma-Aldrich (St. Louis, MO). The complex ECM matrigel purified from the Engelbreth-Holm-Swarm sarcoma of mice has maintained its biological complexity (13,14) and is widely used as a model system for native ECM. ECM and laminin were thawed on ice overnight before use. Collagen IV was dissolved in 0.25% acetic acid (pH 3) for several hours to a final concentration of 3 mg/mL and buffered to pH 7.5 before mixture with laminin or polystyrene particles. 50 mg/ml heparin was dissolved in 10 mM Tris containing 600 mM NaCl (pH 7.5). For experiments, ECM was diluted with MEM-$\alpha$ to a final protein concentration of 4.55 mg/mL. All samples were incubated at their final protein concentrations in presence of the probing particles and (if applicable) rescue agents at 37°C for 30 min to induce gelation. Heparinase I and II from flavobacterium heparinum were dissolved in 20 mM TRIS containing 4 mM $CaCl_2$ and five units were added to each sample of 100 $\mu$L ECM solution before gelation. An additional 30 min of incubation time at 37°C were provided to allow for sufficient enzymatic activity before the samples were analyzed by microscopy.

#### *Polystyrene particles*

Fluorescent polystyrene particles (carboxyl-terminated or amine-terminated) with 1 $\mu$m diameter were obtained from Sigma-Aldrich. Polyethyleneglycol (PEG) coating of 1.1 $\mu$m carboxyl-terminated latex beads (Interfacial Dynamics, Eugene, OR) was performed using a carbodiimide-coupling protocol as outlined in Valentine et al. (15).

#### *Liposomes*

Lipids were obtained from Avanti Polar Lipids (Alabaster, AL) and dissolved in chloroform. Liposomes were prepared from 1,2-dioleoyl-*sn*-glycero-3-phosphocholine (DOPC), 1,2-dioleoyl-3-trimethylammonium-propane (DOTAP), 1,2-dioleoyl-*sn*-glycero-3-[phospho-rac-(1-glycerol)] (DOPG), and fluorescently labeled 1,2-dipalmitoyl-*sn*-glycero-3-phosphoethanolamine-*n*-(Lissamine Rhodamine B Sulfonyl) (Rh-DPPE). Lipids were mixed to a total amount of 0.5 $\mu$mol, solvent evaporation was conducted in vacuum overnight. Dried lipids were resuspended 250 $\mu$M in MEM-$\alpha$ (Minimum Essential Medium Alpha from Invitrogen, Karlsruhe, Germany; salt content: 117 mM NaCl, 26 mM $NaHCO_3$, 5 mM KCl, 1.8 mM $CaCl_2$, 0.8 mM $MgSO_4$) and kept at room temperature for 1 h with occasional vortexing. The suspension was then sonicated in an ultrasonic bath for 30 min to produce small unilamellar vesicles. These were filtered through a 0.2-$\mu$m sterile syringe filter, stored at 4°C, and used within seven days. The liposomes obtained by this protocol had average sizes of $\approx$160–170 nm with polydispersity indices of 0.3–0.4. However, given the drastic differences in the particle mobility (3–4 orders of magnitude, see Results and Discussion), these uncertainties in the liposome size do not significantly influence our results.

### Methods

#### *Particle characterization*

Size and $\zeta$-potential of polystyrene particles and liposomes were determined with dynamic light scattering using a Zetasizer Nano ZS (Malvern Instruments, Herrenberg, Germany). For size and $\zeta$-potential measurements, the lipids were resuspended in 2 mM Tris containing 100 mM NaCl (pH 7.5).

#### *Data acquisition*

Fluorescence or phase contrast images were obtained on an Axiovert 200 microscope (Zeiss, Oberkochen, Germany) with an Achroplan 63× LD 0.75 NA PH2 objective (Zeiss). Images were acquired with a digital camera (ORCA-ER C4742-95; Hamamatsu, Hamamatsu City, Japan) using an image acquisition software developed in our group (OpenBox (16)). The particle position was followed by a tracking algorithm using a two-dimensional Gaussian fit to the particle intensity profile, which resulted in subpixel precision (<5 nm (16)). From the two-dimensional intensity profile, single particles could clearly be distinguished from smaller aggregates (which were not evaluated for the calculation of apparent diffusion constants).

#### *Data analysis*

To quantify the microscopic mobility of the test particles, their apparent diffusion coefficient is determined from the trajectory of motion of the particles. It is important to note that we focus on the short time movement of the particles, i.e., within a time window of 12 s, where geometric hindrance of the particle movement is negligible. In brief, the mean-square displacement (msd)

$$msd(\tau) = \frac{1}{N}\sum_{i=0}^{N}[\boldsymbol{r}(i\Delta t + \tau) - \boldsymbol{r}(i\Delta t)]^2 \quad (1)$$

is related to the diffusion coefficient via $msd(\tau) = 2nD\tau$, where $n = 2$ for the quasi-two-dimensional trajectories $\boldsymbol{r}(t) = (x(t), y(t))$ analyzed here. To avoid artifacts arising from statistical limitations, note that only the first 10% of the $msd(\tau)$ data is used, i.e., up to $\tau = 1.2$ s, to determine diffusion coefficients. In this short time regime, the obtained msd curves are linear and no saturation is observable, confirming that geometric constraints do not play a role on this timescale. Of course, for mobile particles, the diffusive motion at longer timescales will be modified by geometric constraints that are imposed by the architecture of the hydrogel. However, at short timescales or if the particle motion is drastically suppressed by the hydrogel, such geometric hindrance effects at long timescales do not play a role. To validate this methodology, we apply it to PEG-coated particles that are freely floating in water. The obtained diffusion coefficient $D_{PEG}^{H_2 0} = (0.5 \pm 0.1)\ \mu m^2/s$ (see later in Fig. 3) can be related to the viscosity of water $\eta$ using the Einstein relation

$$D = \frac{k_B T}{6\pi\eta R},$$

where $6\pi\eta R$ denotes the friction coefficient for a spherical particle with radius $R$. We obtain $\eta = 0.9$ mPa s, which perfectly matches the viscosity of water at room temperature.

## RESULTS AND DISCUSSION

In hydrogels such as the extracellular matrix (ECM), the mobility of proteins, bacteria, or other microscopic particles is geometrically restricted by the mesh size. The combined density of all participating biopolymers sets this mesh size of the ECM hydrogel. Particles with diameters larger than this mesh size are rejected while smaller particles should, in principle, be able to pass the hydrogel barrier. Thus, for a detailed characterization of the barrier function of the ECM model system studied here, an estimate of this mesh size is crucial. Monodisperse polystyrene (PS) particles are ideal tools to locally probe the mesh size of biological hydrogels. To minimize unspecific interactions with the polymer matrix, a passivation of these particles by coating with the inert PEG has been shown to be important (15). The diffusive motion of such a PEG-passivated polystyrene particle of 1.1 $\mu$m size in a reconstituted ECM hydrogel (4.55 mg/mL total protein concentration) is depicted in Fig. 1 *B*. While exploring the ECM hydrogel, the particle travels several meshes that have a typical size of $\approx$2–3 $\mu$m. Note that for higher protein concentrations such as 9.1 mg/mL, the hydrogel mesh size can be determined more accurately with 1.1-$\mu$m-sized particles to be (1.7 $\pm$ 0.3) $\mu$m (data not shown). Thus, for the conditions studied in this article, one might expect that the microscopic mobility of particles with diameters smaller than 2 $\mu$m should be qualitatively comparable to free diffusion. We test this hypothesis by analyzing the microscopic mobility of various particles that differ in size. It is important to note that all particles studied here are significantly smaller than 2 $\mu$m, and thus smaller than the mesh size of the ECM hydrogel. Surprisingly, if the microscopic mobility of nonpassivated carboxyl-terminated polystyrene beads of 1-$\mu$m size is monitored, a massive slowdown of the particle movement is observed (Fig. 2 *A*). The same result is obtained for smaller carboxyl-terminated polystyrene particles of 105-nm or 50-nm size (data not shown) or if DOPG liposomes of $\approx$170 nm size are used (Fig. 2 *B*). Yet, neutral DOPC liposomes ($\approx$160 nm) appear to be just as mobile as the PEG-passivated polystyrene particles. Obviously, negatively charged particles are effectively trapped while neutral particles can easily pass the hydrogel. These results suggest that the surface charge of microscopic particles regulates their diffusive mobility in the ECM hydrogel. So far, the particles showing suppressed diffusion all possessed a highly negative surface potential (Fig. 2, *C* and *D*). Thus, one might expect that the ECM hydrogel selectively traps negatively charged particles while neutral and positively charged particles are allowed to pass. Yet, the microscopic mobility of positively charged particles is affected in a similar way: amine-terminated polystyrene particles (1 $\mu$m) as well as DOTAP liposomes ($\approx$165 nm) are effectively trapped in the gel (Fig. 2, *A* and *B*), even though the surface potential of the amine-particles is rather low (Fig. 2 *C*).

These results clearly demonstrate that the suppressed mobility of microscopic particles in ECM cannot primarily arise from the steric effects imposed by the polymer matrix: the actual size of the particles seems not to play an important role since all particles tested here are smaller than the mesh size of the hydrogel anyway. Instead, the effective filtering of small particles by ECM hydrogels seems to originate from the electrostatic interaction of the particle surface charge with the polymers, for both algebraic signs of the particle charge.

To quantify the observed stickiness of the trapped particles, an impartial parameter is needed that describes the strength of the remaining diffusive motion. For diffusing particles, the trajectory of motion can be employed to calculate an apparent diffusion coefficient $D$ (see Materials and Methods), which is a direct measure for the microscopic mobility of the particle. We now aim to quantitatively relate this apparent diffusion coefficient to the surface charge of the particles. The $\zeta$-potential of colloidal particles is a well-established parameter, which can be used to characterize their electrostatic surface properties. Liposomes offer the possibility to gradually tune their surface charge by varying the mixture ratio of different lipids, i.e., lipids with neutral, positively charged, or negatively charged headgroups. The easy control over their size and surface functionalization as well as their attractive biological properties has made them widely used tools in biomedical applications (17,18). In this study, different mixtures of DOPC (zwitterionic = neutral), DOTAP (positively charged), and DOPG (negatively charged) are chosen to create particles that cover a broad range of surface charges (see Fig. 3, *B* and *C*) but have a similar size of $\approx$160–170 nm. In Fig. 3 *B*, the offset of the negative/positive boundary toward low DOTAP contents arises from the presence of 5 mol % negatively charged Rhodamine-DPPE, which is

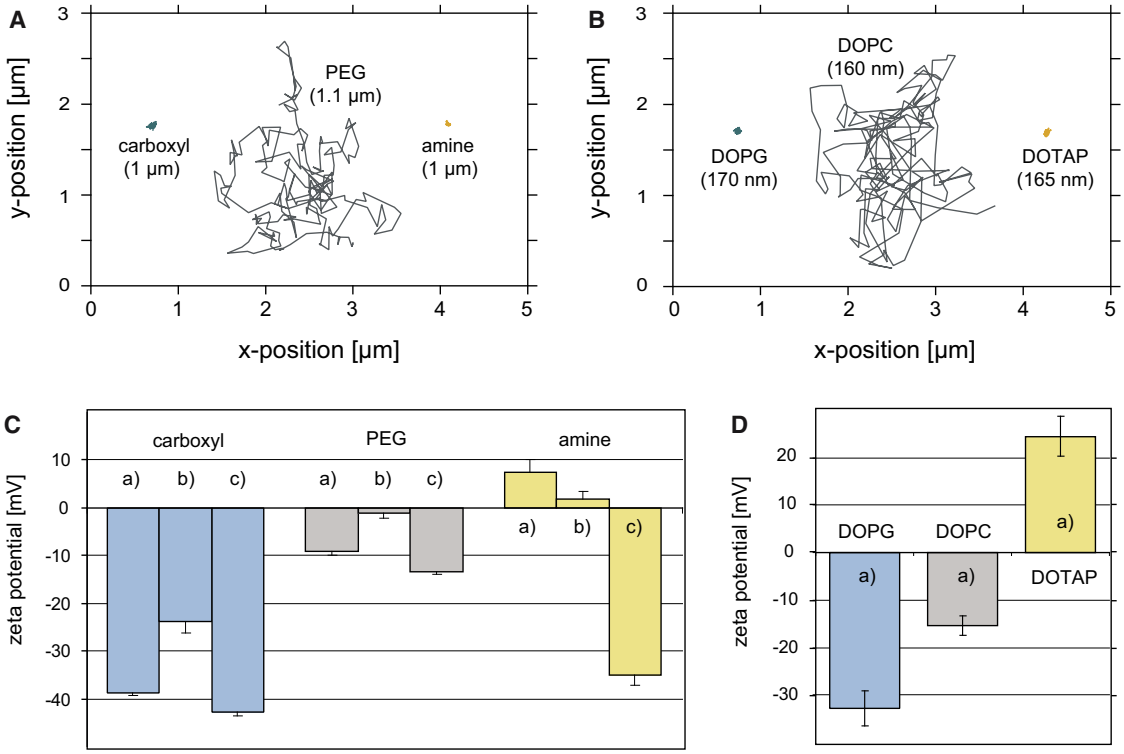


FIGURE 2 Particle mobility and particle surface charge are correlated. (*A*) Trajectories of polystyrene particles (1 $\mu$m and 1.1 $\mu$m in size) with different surface modifications. The diffusive motion of amine- and carboxyl-terminated particles is strongly suppressed in ECM hydrogels; however, PEG-coated carboxyl-particles can diffuse mostly unhindered. (*B*) Trajectories of liposomes (~160–170 nm in size) with different lipid compositions. DOPG/Rh-DPPE and DOTAP/Rh-DPPE liposomes are effectively trapped while DOPC/Rh-DPPE liposomes can diffuse freely. The time range for the data shown in panels *A* and *B* is 12 s each. (*C* and *D*) Zeta potential of the particles shown in panels *A* and *B* as determined in (*a*) 2 mM Tris buffer containing 100 mM NaCl (pH 7.5) and additional (*b*) 1 M KCl or (*c*) 0.5 mM heparin, respectively.

used to fluorescently label the liposomes. The sigmoid dependence of the $\zeta$-potential at small DOTAP and DOPG contents, respectively, is probably due to a nonideal zwitterionic behavior of the DOPC lipids, which is induced by the charged headgroups of neighboring lipids.

For moderate DOPG and DOTAP contents these liposome particles exhibit quasi-free diffusive motion with apparent diffusion coefficients between 0.15 and 0.33 $\mu m^2/s$ (Fig. 3 *A*), which is ~10-fold smaller than expected for free diffusion in water. However, at DOTAP contents $\geq$30%, a sudden and drastic drop in the apparent diffusion coefficient by three orders of magnitude down to $<0.0001$ $\mu m^2/s$ is observed, which nicely confirms the direct correlation of particle surface charge and microscopic mobility. Consistently, for the negatively charged DOPG liposomes, a similar breakdown of the microscopic particle mobility occurs, yet at much larger DOPG contents of $\approx$60% (Fig. 3 *A*). This breakdown of the particle mobility is drastic and complete. When samples with $\geq$30% DOTAP or >60% DOPG are thoroughly screened under the microscope by eye, there are no mobile particles detectable. Accordingly, a quantitative analysis of the corresponding particle trajectories yields extremely low diffusion coefficient values, which are close to the resolution limit of our microscopy setup. These experiments on the microscopic mobility of liposomes also demonstrate that the described effects are independent of the (bio)chemical origin of the charge as polystyrene particles and liposomes behave identically—provided their surface charges are comparable. In detail, the $\zeta$-potentials of the carboxylated PS particles ($\zeta_{carboxyl}$ = (–38.8 $\pm$ 0.6) mV) and the amine-terminated PS particles ($\zeta_{amine}$ = (7.4 $\pm$ 2.6) mV) are located in the immobile regime of Fig. 3 *A* while the PEG-passivated particles ($\zeta_{PEG}$ = (–9.1 $\geq$ 0.8) mV) are clearly situated in the mobile charge window. Surprisingly, this charge window has very steep edges, and a sharp transition from a regime of quasi-free mobility to a regime of almost complete immobilization is observed (*red lines* in Fig. 3 *A*). We never detect particles showing an intermediate diffusion behavior. The high sensitivity of the microscopic particle mobility on the surface charge of the particle becomes evident when the diffusion behavior of the 60% DOPG liposomes is analyzed in detail. For this particular particle species, the diffusion coefficient distribution reveals two well-defined subpopulations as represented by the black and white bar in Fig. 3 *A*—corresponding to the mobile and immobile regimes discussed before. Because mobile and immobile particles can be found in close neighborhood, this suggests that, at this mixture ratio, small fluctuations in the liposome composition occurring

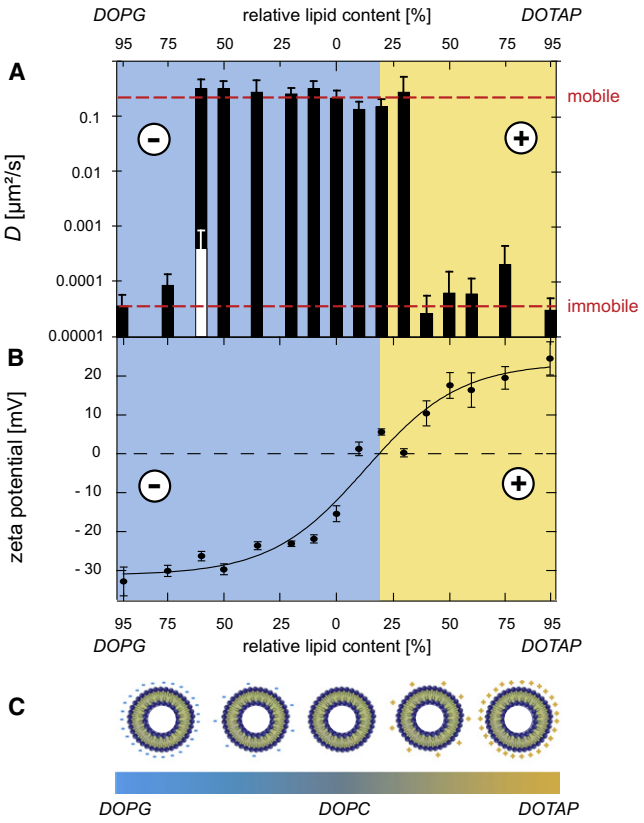


FIGURE 3 The extracellular matrix constitutes an electrostatic bandpass. (*A*) Depending on the particular lipid mixture, the microscopic mobility of the liposome particles drastically varies: a bandpass behavior with respect to the surface charge is observed. A mobile and an immobile regime emerge. The dashed red lines represent the two distinct levels of mobility as described in the main text. Liposomes at various sample positions are analyzed; the error bars show the standard deviation characterizing the distribution of the obtained diffusion constant values. The white bar at 60% DOPG represents an immobile subpopulation as described in the main text. (*B*) The surface potential of liposomes can be gradually varied by changing the lipid content. The error bars represent the standard deviation as determined from triple measurements. (*C*) Schematic representation of different liposome populations with varying lipid composition and surface charge.

during the particle preparation are sufficient to cross the critical surface charge threshold, which allows for local diffusion. This finding in combination with the sharp mobile/immobile transition at both sides of the charge axis demonstrates the high sensitivity of the microscopic filter mechanism, which is established by the extracellular matrix.

To further characterize this microscopic filter mechanism, it would be helpful if the mobility of the trapped particles could be rescued. Such an experiment would give important insights into the microscopic principles guiding the selective filter mechanism of ECM hydrogels. As discussed before, the drastic difference in the local diffusion behavior of small particles in the multicomponent ECM hydrogel is directly correlated with the surface charge of the particles. In salt buffer, the surface charge of synthetic particles or biomolecules is partially shielded by solubilized ions that form thin shells of counter charges around the charged molecule. This Debye screening becomes more pronounced with increasing salt concentrations. A similar strategy might be applicable for weakening the attractive interaction between charged particles and the ECM hydrogel.

Due to their robustness against changes in the buffer conditions, we conduct such a mobility rescue experiment with polystyrene particles instead of liposomes. We investigate the microscopic mobility of these polystyrene particles in the presence of two putative rescue agents, i.e., at high concentrations of KCl and with small amounts of heparin. The addition of 1 M KCl to the MEM-$\alpha$ buffer has a drastic effect on the mobility of the formerly trapped amine- and carboxyl-terminated particles: Both particle types show significantly enhanced mobility (Fig. 4) compared to standard buffer conditions in MEM-$\alpha$ ($\approx$150 mM total salt concentration, see Materials and Methods). To visualize the heterogeneity of this effect, it is helpful to compare the distribution of the apparent diffusion coefficients with and without the addition of 1 M KCl. While at standard salt concentrations, the distribution is rather homogeneous, the local diffusion coefficients obtained in presence of 1 M KCl cover a range of almost four orders of magnitude—for both the amine-terminated and the carboxyl-terminated particles. In contrast, the microscopic mobility of the PEG-passivated particles is largely insensitive to the change in salt concentration. These findings correlate with the alterations in the effective surface potentials of the particles. In free solution, the addition of 1 M KCl partially shields the $\zeta$-potential of all particles (Fig. 2 *C*). In detail, the surface potential of the carboxyl-terminated particles becomes significantly more positive, from $\zeta_{\mathrm{carboxyl}} = (-38.8 \pm 0.6)\mathrm{mV}$ to $\zeta^{\mathrm{KCl}}_{\mathrm{carboxyl}} = (-23.7 \pm 2.4)\mathrm{mV}$, while the $\zeta$-potential of the amine-terminated particles is reduced from $\zeta_{\mathrm{amine}} = (7.4 \pm 2.6)\mathrm{mV}$ to $\zeta^{\mathrm{KCl}}_{\mathrm{amine}} = (1.8 \pm 1.5)\mathrm{mV}$, shifting both particle species inside the mobility window. In contrast, the surface potential of the PEG-passivated particles is always located in this mobility window, be it with ($\zeta^{\mathrm{KCl}}_{\mathrm{PEG}} = (-1.0 \pm 1.2)\mathrm{mV}$) or without the addition of 1 M KC1 ($\zeta_{\mathrm{PEG}} = (-9.1 \pm 0.8)\mathrm{mV}$).

These findings clearly demonstrate the electrostatic and local nature of the microscopic filtering mechanism of the ECM. It also nicely shows that other possible contributions, such as hydrophobic interactions between the particles and the hydrogel, play only a secondary role.

For living organisms it is crucial that this filter mechanism in the extracellular space can be locally tuned, e.g., if proteins stored in the extracellular space shall be released on demand. It has been shown that the microscopic mobility of lactoferrin in the extracellular space of rat brains can be enhanced by the blood coagulant heparin (19). It is thought that many proteins possess putative heparin-binding sites, i.e., clusters of positively charged amino acids that interact specifically with the negatively charged glucosaminoglycan groups of heparin (20); similar specific interactions are also proposed for heparan sulfate chains (21). In the well-defined model system

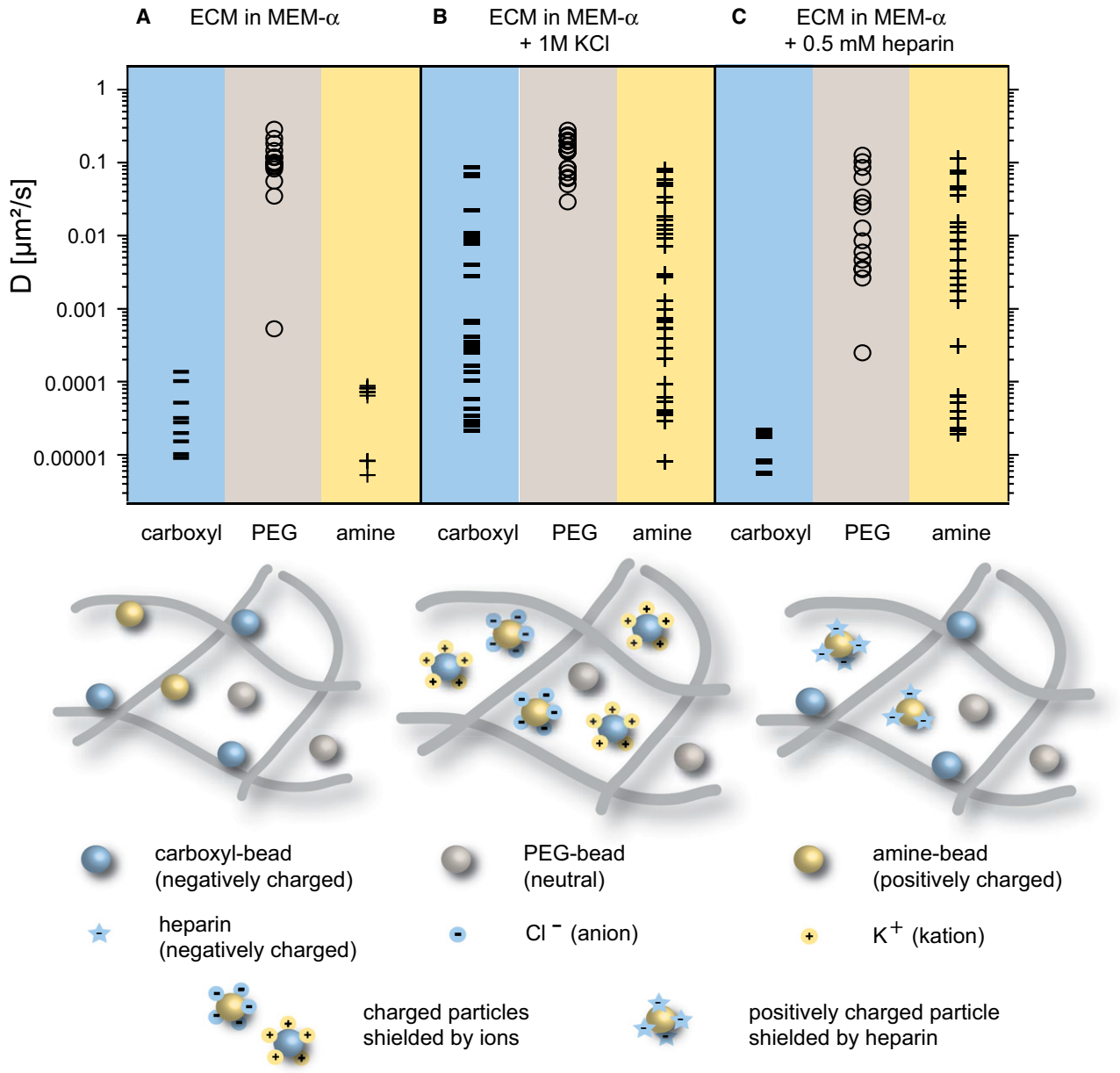


FIGURE 4 Local heterogeneity and rescue of the microscopic mobility. (*Upper panel*) Particles at various sample positions are analyzed to characterize the distribution of the local mobility properties in ECM with and without a rescue agent. (*A*) In standard MEM-α buffer, the distribution width of the diffusion constant is quite narrow for both mobile and immobile polystyrene particles. (*B*) The mobility of the trapped particles can be rescued by adding 1 M KCl resulting in a very broad distribution of local diffusion coefficients. PEG-passivated particles are unaffected by the addition of 1 M KCl. (*C*) 0.5 mM heparin can rescue the mobility of the positively charged amine-particles, but not the mobility of the negatively charged carboxyl-particles. (*Lower panel*) Schematic representation of mobile and immobile particles at different conditions. At high salt concentrations, ions weaken the electrostatic interaction of the charged particles (*yellow*, *blue*) with the hydrogel biopolymers by Debye screening. Heparin (*blue star*) neutralizes the surface charge of amine-beads (*yellow*) and thus rescues their mobility.

studied here, the addition of small amounts (0.5 mM) of heparin has, indeed, a strong effect on the microscopic particle mobility in ECM hydrogels. Similar to the charge screening by high salt concentrations, the mobility of the amine-terminated particles can be rescued and a broad distribution of apparent diffusion coefficients emerges (Fig. 4). However, this effect is not symmetric with respect to the algebraic sign of the particle surface charge: negatively charged carboxyl-terminated particles are unaffected by the addition of heparin and remain trapped. It is important to note that the small amount of added heparin is not sufficient to generally screen the electrostatic interaction in ECM hydrogels, which accounts for its ineffectiveness toward the mobility of negatively charged particles. Instead, unspecific absorbance of heparin molecules to the surface of the amine-terminated particles may be a similarly efficient mechanism for

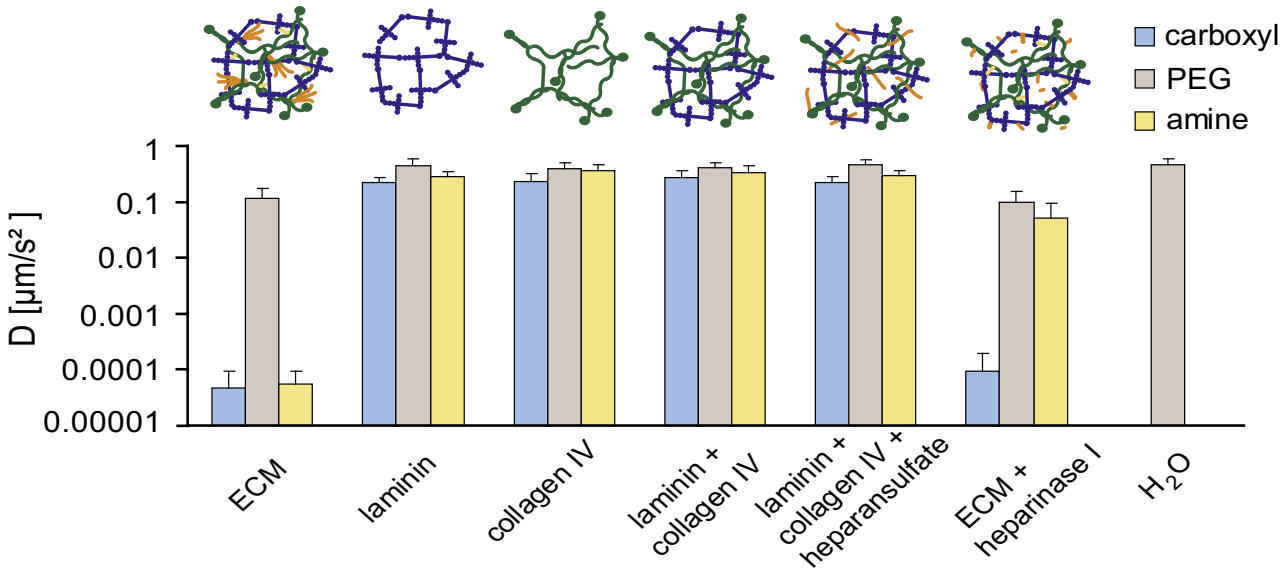


FIGURE 5 Quantification of the microscopic mobility of the tracer particles in different environments. For each experimental condition, various positions in the hydrogel are analyzed. The bars represent the mean diffusion coefficients, and the error bars denote the standard deviations. In ECM, the diffusion coefficient is reduced > 1000fold to virtually zero for both positively charged amine-terminated and negatively charged carboxyl-terminated particles. PEG-passivated particles, however, exhibit an apparent diffusion constant that is only fourfold smaller than the respective value in pure water. Such a drastic suppression of the particle mobility is observable neither in pure laminin or pure collagen IV hydrogels nor in mixed laminin/collagen IV hydrogels. The bandpass filtering is lost if heparan sulfate is enzymatically digested from the perlecan complex by heparinase I. Conversely, the bandpass filtering is not observable if free heparan sulfate chains are added to the mixed laminin/collagen IV hydrogel.

shielding the surface charge of the particles. Indeed, in free solution, the surface potential of all particle species becomes significantly more negative in the presence of 0.5 mM heparin: $\zeta^{\text{heparin}}_{\text{carboxyl}} = (-42.7 \pm 1.0)\text{mV}$, $\zeta^{\text{heparin}}_{\text{PEG}} = (-13.3 \pm 0.6)\text{mV}$, and $\zeta^{\text{heparin}}_{\text{amine}} = (-35.0 \pm 2.2)\text{mV}$ (see Fig. 2 *C*). Clearly, this unspecific absorption effect will be less drastic in the presence of the ECM hydrogel where heparin might also unspecifically bind to the hydrogel polymers. Still, it seems to be efficient enough to shift the formerly positively charged amine-particles into the mobile regime of the charge bandpass.

Having demonstrated that the interaction between filtered particles and the ECM hydrogel is based on elecrostatic effects, we finally try to address the question of which component of the ECM mainly dictates its filtering properties. The extracellular matrix is a complex system; the ECM hydrogel investigated so far has been purified from the Engelbreth-Holm-Swarm sarcoma of mice, and thus has maintained its biological complexity. As discussed before, it is mainly constituted by the three biopolymers: laminin, collagen IV, and perlecan. Small amounts of the molecule nidogen act as cross-linking agents between these three biopolymer systems. In vitro reconstitutions of extracellular hydrogels, however, often employ only one biopolymer (22,23) or two-component mixtures (24), and thus might not appropriately reflect the microscopic barrier function of the native ECM.

Interestingly, in reconstituted single-component hydrogels, which contain either 1 mg/mL laminin or 1.5 mg/mL collagen IV only, the drastic suppression of the microscopic particle mobility observed for the multicomponent ECM does not occur (Fig. 5). In contrast, the mobility of all particles is independent of the surface properties of the tracer particles and comparable to free diffusion in water. Identical results are obtained if laminin and collagen IV are mixed (i.e., 0.5 mg/mL laminin and 0.27 mg/mL collagen IV reflecting the relative biopolymer content of laminin and collagen IV in native ECM) to form a two-component hydrogel (Fig. 5). This demonstrates that neither laminin nor collagen IV alone can reproduce the microscopic filter effect of the ECM. Instead, heparan sulfate molecules, which are attached to the biopolymer network in the extracellular space, might be vital for the microscopic barrier function and filter effect of the ECM. Heparan sulfate is a strongly anionic linear polymer of uronic acid and glucosamine disaccharide units, very similar to the blood coagulant heparin. It has already been proposed that heparan sulfate molecules can regulate the distribution of proteins within the extracellular space (19). In vivo experiments have shown that heparin can cause a barrier dysfunction in the subendothelial matrix, which can be traced back to a loss of heparan sulfate (25). Consistently, a similar weakening of the ECM barrier function is observed in tissue if heparan sulfate is removed from the ECM layer of the basement membrane by enzymatic digestion (12). We now aim to unravel the contribution of heparan sulfate chains to the barrier function of the ECM hydrogel in our in vitro assay. As depicted in Fig. 5, the bandpass filtering of the ECM hydrogel is lost if the heparan

sulfate chains are enzymatically digested from the native multicomponent ECM hydrogel by heparinase I; virtually identical results are obtained with heparinase II (data not shown). Interestingly, the barrier function of the hydrogel toward the negatively charged polystyrene particles persists even if the heparan sulfate chains are degraded. This suggests that either the protein core of the perlecan complex or the nidogen molecules are responsible for the filtering of negatively charged particles. Conversely, the addition of 4.5% (w/w) heparan sulfate chains (representing the relative heparan sulfate content in native ECM) to the two-component laminin/collagen IV hydrogel described before is not sufficient to establish the bandpass filtering which is observed for the native ECM hydrogel (Fig. 5). Even larger concentrations of heparan sulfate chains cannot establish a perceivable filtering effect (data not shown). At this point, it is important to note that heparan sulfate cannot bind itself to laminin or collagen IV. This suggests that a fixation of the charged heparan sulfate chains to the protein matrix of the hydrogel is crucial for the creation of an effective charge filter. Such a fixation can be accomplished by the protein core of the perlecan complex (26), which is lacking in our simplified reconstituted system.

In summary, our results clearly demonstrate that simple model systems of the extracellular matrix are insufficient in reproducing the microscopic barrier function of the ECM. A high level of biological complexity is indispensible to achieve the sensitive filtering function that is established by the ECM. For instance, the strongly charged heparan sulfate chains that are attached to the laminin/collagen IV network of the hydrogel are essential for the microscopic filtering process of the ECM, although they are not sufficient.

Whereas, until now, the mobility of particles within the ECM was regarded to be mainly dictated by the density of biopolymers and the overall charge of the hydrogel, here we have identified the highly localized character of the interaction of the particles with the ECM constituents to be pivotal. The results presented in this study can be summarized in a simple biophysical model for the electrostatic barrier function of the ECM (Fig. 6). The complex ECM hydrogel can be interpreted as a network with localized charge patches of either algebraic signs. The key player bearing the negative charge is heparan sulfate; the positive charge may be localized in the protein core of the perlecan complex or in the nidogen molecules. This local distribution of different charge traps gives rise to the electrostatic bandpass behavior reported here. Geometric hindrance effects that are imposed by the detailed structural organization of the ECM only play a minor role for the mobility of submicron particles within the hydrogel. Their surface charge, however, is the key parameter in determining the microscopic mobility of the particles—causing either free passage through the ECM layer or rigorous restriction.

The correct organization and functionality of the basal lamina is crucial for correct angiogenesis; defects in the composition of the ECM can cause severe diseases (3,27). On the other hand, cells rely on the controlled storage and release of growth factors by the extracellular matrix (5,28). In tumor tissue, this microscopic filtering process is malfunctioning, giving rise to a decrease in the microscopic mobility of particles (1,29). The high sensitivity of the filter mechanism described here not only demonstrates that the composition of the ECM has to be tightly regulated, it also gives rise to a delicate tunability of the microscopic mobility of proteins in vivo. Small modulations of the surface charge of proteins by phosphorylation (charge generation) or methylation (charge depletion) might be sufficient to activate or disable the mobility of small proteins or macromolecules on demand. Furthermore, moderate alterations in the pH-conditions of the extracellular space might change the degree of protonation of the ECM biopolymers and with that, their state of charge. At the same time, such changes in the $H^+$ concentration could also significantly affect the electrostatic screening of particle surface charges. Similarly, increased levels of extracellular salt concentrations can also efficiently contribute to release trapped/stored molecules on demand. Finally, the formation of electrostatically neutral complexes by transport mediators such as heparin can specifically activate the microscopic mobility of particles. A similar strategy is already exploited for delivering highly

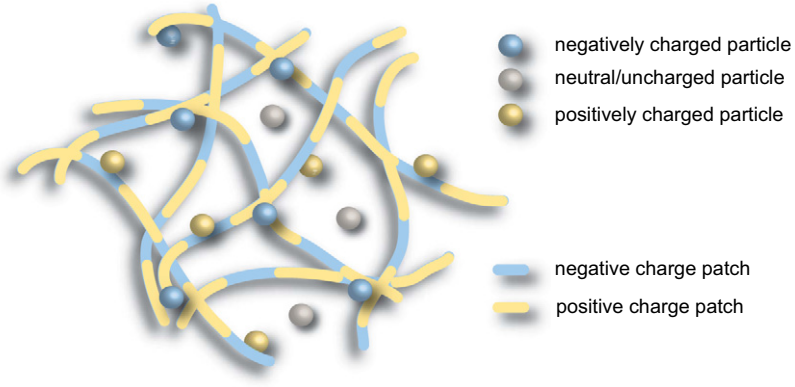


FIGURE 6 Biophysical model for the filtering function of the extracellular matrix: The ECM can be represented as a hydrogel with local patches of either positive or negative charge. In this patchworklike hydrogel, charged particles (*yellow*, *blue*) are trapped in the respective region of opposite charge (*blue*, *yellow*), while neutral particles (*gray*) can diffuse nearly unhindered.

negatively charged DNA to the airway epithelium of mice, to penetrate the mucus hydrogel barrier (30). Thus, we speculate that the microscopic filter principles elucidated here might be more general, and could also be applicable to other biological hydrogel barriers such as the mucus layer or the nuclear core complex.

We thank Katharina Ribbeck for helpful suggestions and discussions.

The authors gratefully acknowledge the financial support of the German Excellence Initiatives via the Nanoinitiative Munich and the Munich-Centre for Advanced Photonics. O.L. acknowledges a postdoctoral fellowship from the German Academic Exchange Service.

## REFERENCES

1. Zamecnik, J., L. Vargova, A. Homola, R. Kodet, and E. Sykova. 2003. Extracellular matrix glycoproteins and diffusion barriers in human astrocytic tumors. *Neuropathol. Appl. Neurobiol.* 30:338–350.
2. Kalluri, R. 2003. Basement membranes: structure, assembly and role in tumor angiogenesis. *Nat. Rev. Cancer.* 3:422–433.
3. Schittny, J. C., and P. D. Yurchenco. 1989. Basement membranes: molecular organization and function in development and disease. *Curr. Opin. Cell Biol.* 1:983–988.
4. Rosso, F., A. Giordano, M. Barbarisi, and A. Barbarisi. 2004. From cell-ECM interactions to tissue engineering. *J. Cell. Physiol.* 199:174–180.
5. Taipale, J., and J. Keski-Oja. 1997. Growth factors in the extracellular matrix. *FASEB J.* 11:51–59.
6. Wang, X., R. E. Harris, L. J. Bayston, H. L. Ashe, and I. V. Type. 2008. Collagens regulate BMP signaling in *Drosophila*. *Nature.* 455:72–77.
7. Yuan, F., M. Dellian, D. Fukumura, M. Leunig, D. A. Berk, et al. 1995. Vascular-permeability in a human tumor xenograft—molecular-size dependence and cutoff size. *Cancer Res.* 55:3752–3756.
8. Hobbs, S. K., W. L. Monsky, F. Yuan, W. G. Roberts, L. Griffith, et al. 1998. Regulation of transport pathways in tumor vessels: role of tumor type and microenvironment. *Proc. Natl. Acad. Sci. USA.* 95:4607–4612.
9. Pluen, A., Y. Boucher, S. Ramanujan, T. D. McKee, T. Gohongi, et al. 2001. Role of tumor-host interactions in interstitial diffusion of macromolecules: cranial vs. subcutaneous tumors. *Proc. Natl. Acad. Sci. USA.* 98:4628–4633.
10. Juillerat-Jeanneret, L. 2008. The targeted delivery of cancer drugs across the blood-brain-barrier: chemical modifications of drugs or drug-nanoparticles? *Drug Discov. Today.* 13:1099–1106.
11. Kostarelos, K., D. Emfietzoglou, A. Papakostas, W.-H. Yang, A. Ballangrud, et al. 2004. Binding and interstitial penetration of liposomes within avascular tumor spheroids. *Int. J. Cancer.* 112:713–721.
12. Kanwar, Y. S., A. Linker, and M. G. Farquhar. 1980. Increased permeability of the glomerular basement membrane to ferritin after removal of glycosaminoglycans (heparan sulfate) by enzyme digestion. *J. Cell Biol.* 86:688–693.
13. Kleinman, H. K., M. L. McGarvey, L. A. Liotta, P. G. Robey, K. Tryggvason, et al. 1982. Isolation and characterization of type IV procollagen, laminin and heparan sulfate proteoglycan from the EHS sarcoma. *Biochemistry.* 21:6188–6193.
14. Kleinman, H. K., M. L. McGarvey, J. R. Hassell, V. L. Star, F. B. Cannon, et al. 1986. Basement membrane complexes with biological activity. *Biochemistry.* 25:312–318.
15. Valentine, M. T., Z. E. Perlman, M. L. Gardel, J. H. Shin, P. Matsudaira, et al. 2004. Colloid surface chemistry critically affects multiple particle tracking measurements of biomaterials. *Biophys. J.* 86:4004–4014.
16. Schilling, J., E. Sackmann, and A. R. Bausch. 2004. Digital imaging processing for biophysical applications. *Rev. Sci. Instrum.* 75:2822–2827.
17. Lasic, D. D., and D. Papahadjopoulos. 1998. Medical Applications of Liposomes. Elsevier, Amsterdam, The Netherlands.
18. Torchilin, V. P. 2005. Recent advances with liposomes as pharmaceutical carriers. *Nat. Rev. Drug Discov.* 4:145–160.
19. Thorne, R. B., A. Lakkaraju, E. Rodriguez-Boulan, and C. Nicholson. 2008. In vivo diffusion of lactoferrin in brain extracellular space is regulated by interactions with heparan sulfate. *Proc. Natl. Acad. Sci. USA.* 105:8416–8421.
20. Faham, S., R. E. Hileman, J. R. Fromm, R. J. Linhardt, and D. C. Rees. 1996. Heparin structure and interactions with basic fibroblast growth factor. *Science.* 271:1116–1120.
21. Kreuger, J., D. Spillmann, J.-P. Li, and U. Lindahl. 2006. Interactions between heparan sulfate and proteins: the concept of specificity. *J. Cell Biol.* 174:323–327.
22. Ramanujan, S., A. Pluen, T. D. McKee, E. B. Brown, Y. Boucher, et al. 2002. Diffusion and convection in collagen gels: implications for transport in the tumor interstitium. *Biophys. J.* 83:1650–1660.
23. Erikson, A., H. N. Andersen, S. N. Naess, P. Sikorski, and C. de Lange Davies. 2007. Physical and chemical modifications of collagen gels. *Biopolymers.* 89:135–143.
24. Kuntz, R. M., and W. M. Saltzmann. 1997. Neutrophil motility in extracellular matrix gels: mesh size and adhesion affect speed of migration. *Biophys. J.* 72:1472–1480.
25. Guretzki, H. J., E. Schleicher, K. D. Gerbitz, and B. Olgemoller. 1994. Heparin induces endothelial extracellular matrix alterations and barrier dysfunctions. *Am. J. Physiol. Cell Physiol.* 267:946–954.
26. Iozzo, R. V., I. R. Cohen, S. Grässel, and A. D. Murdoch. 1994. The biology of perlecan: the multifaceted heparan sulfate proteoglycan of basement membranes and pericellular matrices. *Biochem. J.* 302:625–639.
27. Hudson, B. G., S. T. Reeders, and K. Tryggvason. 1993. Type IV collagen: structure, gene organization, and role in human diseases. Molecular basis of Goodpasture and Alport syndromes and diffuse leiomyomatosis. *J. Biol. Chem.* 268:26033–26036.
28. Dowd, C. J., C. L. Cooney, and M. A. Nugent. 1999. Heparan sulfate mediates bFGF transport through basement membrane by diffusion with rapid reversible binding. *J. Biol. Chem.* 274:5236–5244.
29. Magzoub, M., S. Jin, and A. S. Verkman. 2008. Enhanced macromolecular diffusion deep in tumors after enzymatic digestion of extracellular matrix collagen and its associated proteoglycan decorin. *FASEB J.* 278:276–284.
30. Rudolph, C., U. Schillinger, A. Ortiz, C. Plank, M. M. Golas, et al. 2005. Aerosolized nanogram quantities of plasmid DNA mediate highly efficient gene delivery to mouse airway epithelium. *Mol. Ther.* 12:493–501.